

# Significant modification of the surface morphology of polylactide (PLA) and PLA-halloysite nanocomposites in the presence of *N,N'*-ethylenebis(stearamide) upon thermal treatment

M. Pluta<sup>1\*</sup>, J. Bojda<sup>1</sup>, T. Makowski<sup>1</sup>, E. Piorkowska<sup>1</sup>, M. Murariu<sup>2</sup>, L. Bonnaud<sup>2</sup>, P. Dubois<sup>2</sup>

<sup>1</sup>Centre of Molecular and Macromolecular Studies, Polish Academy of Sciences, Sienkiewicza 112, 90-363 Lodz, Poland

<sup>2</sup>Center of Innovation and Research in Materials & Polymers (CIRMAP), Laboratory of Polymeric and Composite Materials (LPCM), University of Mons (UMONS) & Materia Nova Materials R&D Center, Place du Parc 20, 7000 Mons, Belgium

Received 15 April 2020; accepted in revised form 27 May 2020

**Abstract.** Surface morphology and bulk structure of polylactide (PLA) modified with halloysite nanotubes (HNT) treated with *N,N'*-ethylenebis(stearamide) (EBS) and untreated, as well as reference materials – PLA, EBS, and a blend of PLA with EBS, were examined. HNT is known to improve PLA properties, including mechanical and barrier properties. The materials were cold crystallized and tested using DSC, TGA, PLM, SALS, SEM, AFM. The additives affected nucleation and crystallization of PLA, but did not influence crystallinity, which was of approx. 37–40 %. In bulk, PLA crystallized in the form of spherulites in all materials. However, on surfaces of EBS-containing materials, a thin EBS layer with domain morphology was found. The EBS layer induced epitaxial crystallization of PLA in the form of parallel stacks of edge-on lamellae, the phenomenon reported for this polymer pair for the first time. It was observed in PLA with EBS modified HNT and in the PLA blend with EBS. Moreover, the EBS layers imparted hydrophobicity to the EBS-containing materials.

**Keywords:** nanocomposites, polylactide, *N,N'*-ethylenebis(stearamide), crystallization, wettability

## 1. Introduction

Poly(lactic acid) or polylactide (PLA), a thermoplastic aliphatic polyester, has recently gained enormous attention because of the increasing concern for the environment. It is not only (bio)degradable under controlled composting conditions, but also can be produced from renewable natural resources by fermentation of polysaccharides or sugars *e.g.* extracted from corn, potatoes or sugar beets [1–4]. In competition with petroleum-based polymers, PLA is one of the most promising (bio)polymers for future developments because of its many advantages like good mechanical performance, processability, biocompatibility, and recyclability [5–9].

Moreover, the physical modification of PLA with selected organic and/or inorganic additives appeared to be a simple and effective way to modulate its properties. This allows us to extend applications of PLA in different fields, ranging from biomedical to sustainable packaging materials, and textile fibers, as well as to more demanding applications in the engineering sectors requiring high-performance materials. For instance, to improve the toughness and ductility, PLA has been modified *e.g.* via route termed ‘rubber toughening’ and plasticization [10–18]. To enhance thermal stability, mechanical, barrier and other properties, PLA has been filled with organo-modified layered silicates [19–22], carbon nanotubes (CNT)

\*Corresponding author, e-mail: [mpluta@cbmm.lodz.pl](mailto:mpluta@cbmm.lodz.pl)  
© BME-PT

and graphene derivatives [23, 24], calcium sulfate [25, 26], calcium carbonate [27], powders of zinc oxide, silver, silica, etc. [28–30]. Furthermore, it is noteworthy mentioning that more recently, increased interest was observed in the study of polymer nanocomposites containing HNT as a nanofiller, while EBS is considered among additives able to modify the properties and dispersion of fillers in different polymer matrices [31–33]. Also, to allow the utilization of PLA in technical applications, many studies are devoted to annealing of PLA items produced by injection molding, extrusion, 3D printing, etc. These thermal treatments, usually carried out in a broad range of temperature, lead to the considerable increase of PLA crystallinity, changes of morphology and to important improvements of the properties of PLA products [34, 35].

In our previous works halloysite nanotubes (HNT) and HNT treated with *N,N'*-ethylenebis(stearamide) (EBS) were selected as additives for the preparation of new (bio)degradable PLA based nanocomposites with specific end-use characteristics and major improvements of properties [36–41]. Halloysite (HNT), naturally occurring aluminosilicate clay, is featured with high rigidity, good tensile and flexural strength, high susceptibility for dispersion in various polymer matrices due to rod-like geometry and interparticle interactions relatively weaker than between other nanoparticles, such as fumed silica, organo-modified layered montmorillonite (o-MMT) and CNTs [42, 43]. HNT is less costly than CNT. Furthermore, recent FTIR studies showed that outer surface siloxane groups of HNT can interact with end hydroxyl groups of PLA via hydrogen bonding [44, 45]. HNT can be considered as ‘nano-support’ with highly developed surface for EBS [38].

EBS was used as an interfacial modifier to enhance the dispersion of HNT in PLA matrix. EBS remained at the PLA/HNT interface and only its excessive fraction was finely dispersed within the PLA matrix [38, 40, 41]. Amide groups (–CONH–) of EBS can interact with hydroxyl groups on the HNT surface, contributing to the better dispersion of the nanofiller. EBS is also known as an effective nucleating agent for PLA [35, 46, 47].

Our two previous works were focused on studies of PLA-based nanocomposites, containing HNT and EBS-treated HNT, and reference samples – neat PLA and blend PLA/EBS, with a defined amorphous and semi-crystalline structure of PLA matrix, respectively.

Their phase structure, crystalline morphology, thermal behavior, viscoelastic and optical properties in relation to composition has been demonstrated [40, 41].

In the current work, the morphology of free surfaces of neat PLA and PLA-based materials with HNT and/or EBS have been examined. The materials were cold-crystallized with free surfaces and studied using polarized light microscopy (PLM), scanning electron microscopy (SEM), atomic force microscopy (AFM), small-angle light scattering (SALS), differential scanning calorimetry (DSC) and thermogravimetric analysis (TGA). Water wettability was investigated as well. The formation of EBS layer on surfaces of EBS-containing materials and its influence *via* epitaxial crystallization on the morphology of the adjacent PLA were evidenced. The EBS layer induced epitaxial crystallization of PLA in the form of parallel stacks of edge-on lamellae. Moreover, the EBS layer imparted hydrophobicity to the materials. It is worth mentioning that materials with a free surface are produced industrially e.g. using extrusion, blow molding, etc.

## 2. Experimental

### 2.1. Materials

Poly(lactide) (PLA) used in the study was commercially available 4032D grade from NatureWorks LLC (Minnetonka, MN). Its weight-average molar mass  $M_w$  of 130 kg/mol and a dispersity  $M_w/M_n$  of 1.3 were determined by size-exclusion chromatography (SEC) with a multi-angle laser light scattering (MALLS) detector in methylene chloride. According to the supplier, D-lactide and residual monomer contents were 1.4 and 0.14%, respectively, whereas the relative viscosity was 3.94.

Halloysite ( $\text{Al}_2\text{Si}_2\text{O}_5(\text{OH})_4 \cdot 2\text{H}_2\text{O}$ ) nanotubes (HNTs) supplied by Sigma–Aldrich (USA) in the powder form were used as a filler. According to the supplier, a nanotube diameter and length ranged from 30 to 70 nm and from 1 to 3  $\mu\text{m}$ , respectively, whereas a surface area, pore-volume, refractive index and density were 64  $\text{m}^2/\text{g}$ , 1.26–1.34  $\text{ml}/\text{g}$ , 1.54, and 2.53  $\text{g}/\text{cm}^3$ , respectively.

*N,N'*-ethylenebis(stearamide), a fatty amide with the linear formula  $[\text{CH}_3(\text{CH}_2)_{16}\text{CONHCH}_2-]_2$  (EBS) having a molar mass of 593.02 g/mol, melting temperature of 141–146 °C, the density of 0.97  $\text{g}/\text{cm}^3$ , was supplied by Sigma–Aldrich (USA). It was used for effective coating of HNT nanotubes to modify their surface properties and dispersion in PLA matrix [38, 40, 41].

## 2.2. Preparation

After drying at 100 °C for 48 h, HNT was dry-mixed with EBS in a laboratory Rondol turbo-mixer, in weight ratio 80:20. Then, the ‘wet-coating’ at 160 °C was carried out in an internal mixer, at first for 5 min at 30 rpm, and then for 15 min at 100 rpm. Prior to melt-compounding in a twin-screw co-rotating extruder (Leistritz ZSE 18 HP-40D, screw diameter ( $D$ ) = 18 mm,  $L$  (length)/ $D$  ratio = 40), all the components, that is PLA, HNT, and EBS-treated HNT were dried overnight at 60 °C. In the same way, the neat PLA and PLA blend with 1.5 wt% of EBS, as reference materials, were prepared. The preparation of nanocomposites was described in detail by us previously [40]. Table 1 shows sample codes and the composition of all materials studied.

For further studies, thin films (0.25–0.3 mm) sandwiched between polyimide Kapton foils were compression molded at 180 °C for 3 min and then solidified between metal plates. To obtain starting quenched films, the compression-molded films, with free upper surfaces, were (1) heated to 180 °C at 30 °C/min and (2) annealed at this temperature for 2 min, and quenched at 30 °C/min to room temperature ( $RT$ ). To obtain final crystalline materials, the quenched films, after being held for 3 min at  $RT$ , were (3) heated to 120 °C at 10 °C/min and annealed at this temperature ( $T_a$ ) for 20 min (cold crystallization completion), and then (4) cooled at 30 °C/min to  $RT$ . This thermal treatment was carried out in a temperature controlled hot stage of the Linkam CSS450 optical shearing system (Waterfield, UK).  $T_a$  of 120 °C was selected because it is close to the end of cold crystallization and below the beginning of the melting of all materials studied [40]. Moreover, the annealing of PLA in the temperature range 100–120 °C is claimed to lead to maximum crystallization rate, resulting in the minimum crystallization half-time ( $t_{1/2}$ ), defined as the time required to attain half of the final crystallinity [48]. The starting quenched films are denoted with ‘q’, e.g. qPLA, while the final

crystallized films with ‘c’, e.g. cPLA. Subsequently, the surfaces were prepared for SEM and AFM analysis by rinsing and etching. As it will be further described, EBS layers were found on surfaces of EBS-containing materials. In order to remove the EBS layers, the EBS-containing films were rinsed for 6 min in a hot isopropanol bath at approx. 78 °C, agitated with a magnetic stirrer. To have more detailed insight into the morphology, the selective etching of amorphous PLA phase was carried out for the rinsed EBS-containing films as well as for neat PLA and P6H, in a solution containing 0.1 wt% sodium hydroxide, 33 vol% distilled water and 67 vol% methyl alcohol [49] for 0.5 h at  $RT$ . The rinsing and etching conditions were determined experimentally.

## 2.3. Characterization

The thermal behavior of the materials was studied using DSC during heating at a rate of 10 °C/min, under a flow of nitrogen (DSC 2920 TA Instruments, New Castle, DE). Thermogravimetric analysis (TGA) was performed using a TGA Q50 (TA Instruments) at a heating rate of 20 °C/min under air flow, from  $RT$  up to 600 °C.

The structure of the films was examined with PLM using Nikon Eclipse E400 equipped with a SANYO VCC-3770P camera.

The morphology of the crystalline films was also investigated using a SALS technique. Hv scattering patterns were recorded using a He-Ne laser with wavelength ( $\lambda$ ) of 632.8 nm.

Free surfaces of all samples were examined using SEM Jeol 5500LV (operating in the high vacuum mode at an accelerating voltage of 10 kV) after sputtering with gold using JFC-1200 fine coater Jeol (Tokyo, Japan).

AFM Nanosurf Flex Axiom with a C3000 controller (Nanosurf AG, Switzerland) equipped with a commercially available rectangular probe (PPP-NCHR Nanosensors) was used to study the film surfaces in a tapping mode under an ambient atmosphere at  $RT$ . 512×512 data points images were recorded. Image analysis was performed using SPIP Image Metrology software (Denmark).

Water contact angle (WCA) measurements were carried out at  $RT$  using a Phoenix-300 goniometer (SEO Surface Electro Optics, Korea). 5±0.05  $\mu$ l drops of distilled water were placed on film surfaces. WCA values were determined using Drop Analysis program.

**Table 1.** Codes and composition of the materials.

Sample code	PLA content [wt%]	HNT content [wt%]	EBS content [wt%]
PLA	100.0	–	–
P6H	94.0	6	–
P6H/C20	92.5	6	1.5
P1.5C	98.5	–	1.5
EBS	–	–	100.0

Average WCA values were calculated from at least 5 measurements of each material.

### 3. Results and discussion

#### 3.1. Thermal properties

DSC heating thermograms of the crystalline PLA-based films and EBS are shown in Figure 1. The thermograms of starting quenched films are also plotted in Figure 1 in order to present the evolution of the cold crystallization process during heating to  $T_a$ , at which the crystallization was finally completed.

The calorimetric parameters are collected in Table 2. The thermograms of cPLA based materials showed weak glass-rubber transition with  $T_g$  from 62.3 to 63.9 °C, while their starting (quenched) counterparts exhibited a more pronounced transition with  $T_g$  lower by 1.3–3.1 °C due to the lack of crystallinity. All q-materials were amorphous, with the exception of qP6H/C20, which showed trace crystallinity developed during cooling due to the synergistic nucleating effect of the additives. The increase of  $T_g$  of c-samples due to crystallinity was also observed by us previously [41], and also by others, especially after annealing [51, 52]. The main melting peaks of the materials with the additives exhibited weak low- or high-temperature shoulders (indicated by arrows in Figure 1). In addition, small endothermic peaks at 143.8 °C were observed for cP6H/C20 and P1.5C due to the melting of EBS component. Generally, the melting enthalpy of PLA matrix was similar for all c-materials, and corresponds to the crystallinity ( $X_c$ ) of 37–40%, showing the weak effect of the composition (Table 2). However, the melting of PLA reflected the cold-crystallization behavior affected by the presence of the additives [40, 41]. The q-materials with the additives showed a decrease of cold

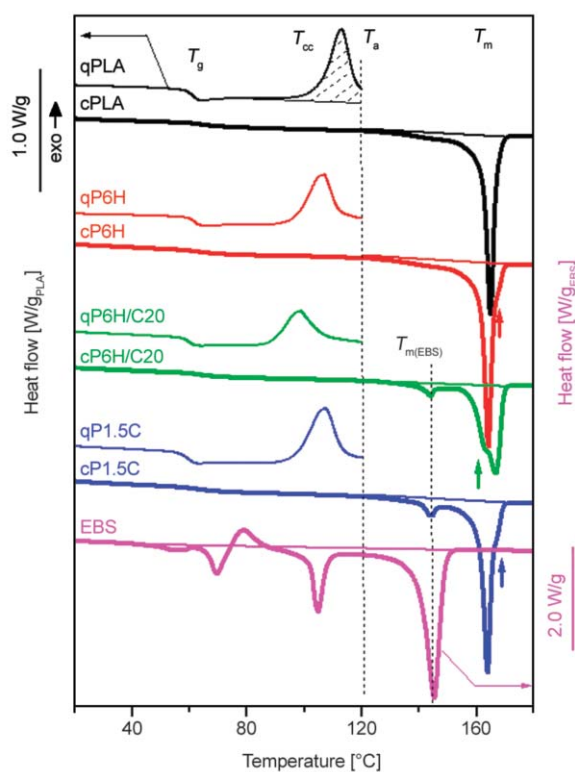


**Figure 1.** DSC heating thermograms (10 °C/min) of PLA based c-materials and EBS (vertically shifted for clarity). The accompanying thermograms show cold crystallization exotherms of the starting q-materials during heating up to  $T_a$  (the dotted part of cold crystallization exotherm of qPLA marks the area integrated for calculation of  $\Delta H_{cc}^q$ ).

crystallization peak rate temperature,  $T_{cc}^q$ , in comparison to neat q-PLA, as shown in Table 2. The ability of HNT and EBS to nucleate crystallization of PLA, and also other polymers was reported previously [47, 53–56]. Generally, the cold crystallization enthalpy,  $\Delta H_{cc}^q$ , was similar for majority q-materials, close to 30, and 26 J/g<sub>PLA</sub> for cP6H/C20 (due to trace crystallinity of the quenched counterpart). However, the

**Table 2.** Calorimetric parameters of starting q- and final c-materials measured during the 1<sup>st</sup> heating at 10 °C/min.  $T_g^c$  and  $T_g^q$  denote the glass transition temperature of c- and q-materials, respectively.  $T_m^c$  and  $\Delta H_m^c$  are the melting peak temperature and melting enthalpy of c-materials.  $T_{cc}^q$  and  $\Delta H_{cc}^q$  are the cold crystallization peak temperature and crystallization enthalpy of q-materials.  $X_c$  is the mass crystallinity of PLA matrix in cPLA-based materials assuming that the heat of fusion of fully crystalline PLA is equal to 106 J/g [50].

Sample code	q-samples (unannealed)			c-samples (annealed)				$\Delta H_{cc}^q/\Delta H_m^c$
	$T_g^q$ [°C]	$T_{cc}^q$ [°C]	$\Delta H_{cc}^q$ [J/g <sub>PLA</sub> ]	$T_g^c$ [°C]	$T_m^c$ [°C]	$\Delta H_m^c$ [J/g <sub>PLA</sub> ]	$X_c$ [wt%]	
PLA	61.4	112.9	30.6	63.9	164.8	41.8	39.4	0.73
P6H	61.7	106.8	30.1	63.0	164.1	44.0	41.5	0.68
P6H/C20	60.2	98.6	26.2	63.3	166.5 143.8*	39.2	37.0	0.66
P1.5C	60.3	107.1	31.6	62.3	163.8 143.8*	42.8	40.4	0.73

\*indicates the effect attributed to EBS

**Table 3.** Calorimetric parameters of EBS measured during the 1<sup>st</sup> heating scan at 10 °C/min.  $T_{m1}$ ,  $T_{m2}$ ,  $T_{m3}$ ,  $T_{m4}$  and  $\Delta H_{m1}$ ,  $\Delta H_{m2}$ ,  $\Delta H_{m3}$  are the melting peak temperatures and corresponding enthalpies, respectively.  $T_{cc}$  and  $\Delta H_{cc}$  denote the cold crystallization peak temperature and enthalpy, respectively.

$T_{m1}$ [°C]	$\Delta H_{m1}$ [J/g]	$T_{m2}$ [°C]	$\Delta H_{m2}$ [J/g]	$T_{cc}$ [°C]	$\Delta H_{cc}$ [J/g]	$T_{m3}$ [°C]	$\Delta H_{m3}$ [J/g]	$T_{m4}$ [°C]	$\Delta H_{m4}$ [J/g]
55.8	9.2	69.5	18.6	78.8	12.4	104.8	51.5	145.2	129.0

crystallization peak shape and temperature depended on the material composition (Table 2, Figure 1). Moreover, it can be estimated that about 70% of the crystallinity of c-materials was formed during heating to  $T_a$  (see ratio  $\Delta H_{cc}^q/\Delta H_{m}^c$ , Table 2).

In turn, EBS exhibited several phase transitions – one crystallization peak at 78.8 °C, three endo-transitions with peaks at 55.8, 69.5, 104.8 °C, and finally a melting peak at 145.2 °C with the corresponding enthalpies listed in Table 3.

The presence of 6 wt% of HNT affected somewhat the thermal stability of PLA; at 6 wt% of HNT content, in air, temperature of 5 wt% loss ( $T_{5\%}$ ) decreased from 342 to 338 °C, whereas, the temperature of maximum degradation rate ( $T_d$ ) increased from 381 to 383 °C, respectively. The addition of 1.5 wt% of EBS to the nanocomposite decreased those temperatures to 307 and 366 °C. However, for P1.5C blend  $T_{5\%}$  and  $T_d$  were higher than for P6H/C20, and were equal to 335 and 374 °C, respectively. Thus, the detrimental effect of EBS on the PLA stability depends on its dispersion and is stronger when EBS remains at the PLA/HNT interface [38, 40, 41]. Nevertheless,  $T_{5\%}$  of all materials studied were well above the temperature range of PLA processing, usually below 200 °C.

## 3.2. Structure

### 3.2.1. PLM

Figure 2 shows PLM micrographs of the morphology of the cPLA materials. q-materials were amorphous, and only qP6H/C20 exhibited a trace of crystallinity. Micrographs of the c-films revealed very fine crystalline aggregates of PLA. When observed by PLM the images of EBS-containing films (Figure 2, bottom) appeared to be slightly brighter. As shown further, this is due to the presence of the EBS crystalline layer on the film surfaces.

### 3.2.2. SALS

Figure 3 shows 2D-SALS Hv patterns of the c-films. The four-leaf clover patterns typical of the spherulitic structure were observed. It follows that the formation

of PLA spherulites during cold crystallization was not disturbed by the additives used.

The average radii of spherulites ( $R_{av}$ ) were calculated based on the 2D-SALS patterns according to Equation (1) [57]:

$$R_{av} = \frac{4.09\lambda}{4\pi \sin\left(\frac{\theta_{max}}{2}\right)} \quad (1)$$

where  $\theta_{max}$  is the angle of the maximum intensity of scattered light at the azimuthal direction of 45°. For 3D spherulites  $R_{av}$  is the fifth-order average; therefore, it is heavily weighted in favor of larger spherulites [58].  $R_{av}$  of 2.11, 1.65, 2.30 and 2.17  $\mu\text{m}$  was calculated for cPLA, cP6H, cP6H/C20 and P1.5C, respectively, indicating a fine spherulitic structure. However, in the case of filled PLAs the actual  $R_{av}$  value may be somewhat affected by isotropic light scattering from micron-sized HNT inclusions seen occasionally in EBS-free nanocomposite (cP6H), as well as from EBS micron domains detected in the blend (cP1.5C) [41].

### 3.2.3. SEM and AFM

Figure 4 demonstrates the SEM micrographs of the free surfaces of the films. The surfaces of neat cPLA and cP6H show a spherulitic structure. However, spherulites seen on the cP6H surface are smaller than those on the neat cPLA surface due to the nucleation activity of HNT. Moreover, the surface of cP6H is rougher than that of cPLA due to the presence of the filler.

Interestingly, the examination of free surfaces of EBS-containing films, cP6H/C20 and cP1.5C, revealed a domain morphology, although their bulk structure was spherulitic as evidenced by SALS. The domains were relatively regular, with a nearly rectangular shape and exhibited shape anisotropy, with length from about 2.1 to 7.0  $\mu\text{m}$  and width of 0.8 to 2.2  $\mu\text{m}$ ; the aspect ratio was noticeably larger for cP6H/C20 than cP1.5C. A similar domain morphology was found on the free surface of neat EBS (Figure 4d, Inset). Hence, it is concluded that the surface of cP6H/C20 and cP1.5C was covered with a thin

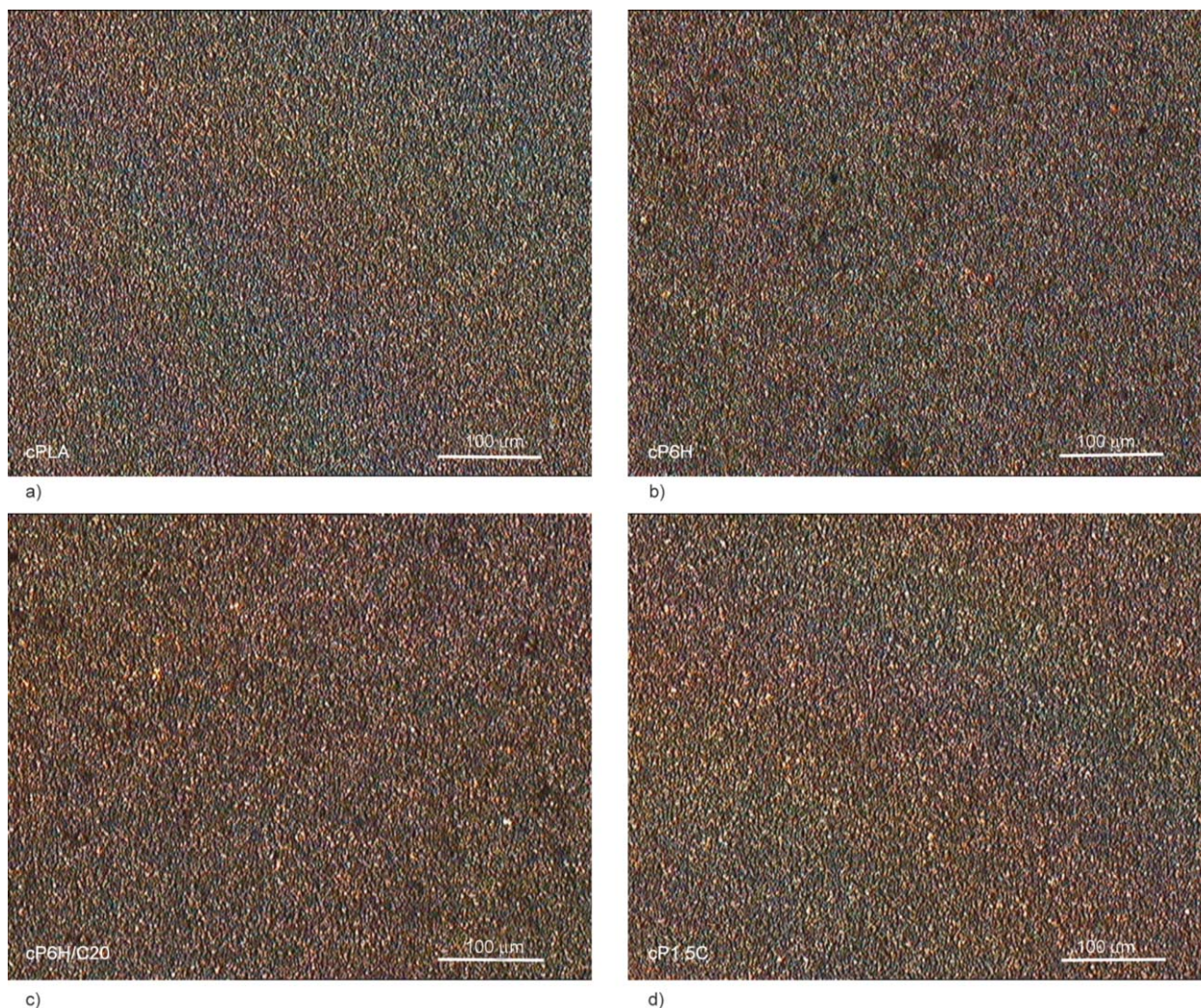


**Figure 2.** PLM micrographs of c-films approx. 20 μm thick: cPLA (a), cP6H (b), cP6H/C20 (c), and cP1.5C (d).

EBS layer. It should be emphasized that a similar EBS layer (*i.e.* with domain morphology) was also observed on the free surface of EBS-containing quenched samples. This implies that cold crystallization of PLA matrix cannot be solely responsible for the formation of the EBS layer. To examine the morphology of PLA surface under the EBS layer, the layer has been removed by rinsing in isopropanol. As verified in a separate experiment, the degree of isopropanol absorption by cP6H/C20 and cP1.5C, was approx. 0.2 and 0.4 wt%, respectively, and did not result in any significant structural changes. Figure 5 displays rinsed surfaces of cP6H/C20 and cP1.5C films, without EBS layers.

On the rinsed surface of cP6H/C20, traces of HNT particles and imprints of removed EBS domains are visible. Distinctly deeper imprints of the EBS domains are seen on the rinsed surface cP1.5C, which suggests that thicker EBS layer formed on cP1.5C than on cP6H/C20. This is possibly due to

the presence of micron-sized EBS inclusions in cP1.5C, whereas in cP6H/C20 EBS was finely dispersed and its fraction was immobilized at the surface of the filler [40]. To have a better insight into the surface morphologies, the EBS-free samples, as well as rinsed cP6H/C20, cP1.5C were etched. Figure 6 presents SEM micrographs of etched surfaces of these films.

Spherulites were visible on the etched surfaces of cPLA and cP6H. In turn, the etched surfaces of rinsed cP6H/C20 and cP1.5C showed a different structure, with stacks of edge-on lamellae densely arranged parallel to each other and size corresponding to sizes of EBS domains, which were previously rinsed out from the surface. It also seems that in cP1.5C the lamellae were parallel to shorter sides of the deep, elongated pockets, seen on the rinsed cP1.5C surface, where thick EBS domains were previously present.

AFM images of the surfaces of cPLA, cP6H, and rinsed cP6H/C20, cP1.5C are shown in Figure 7. The

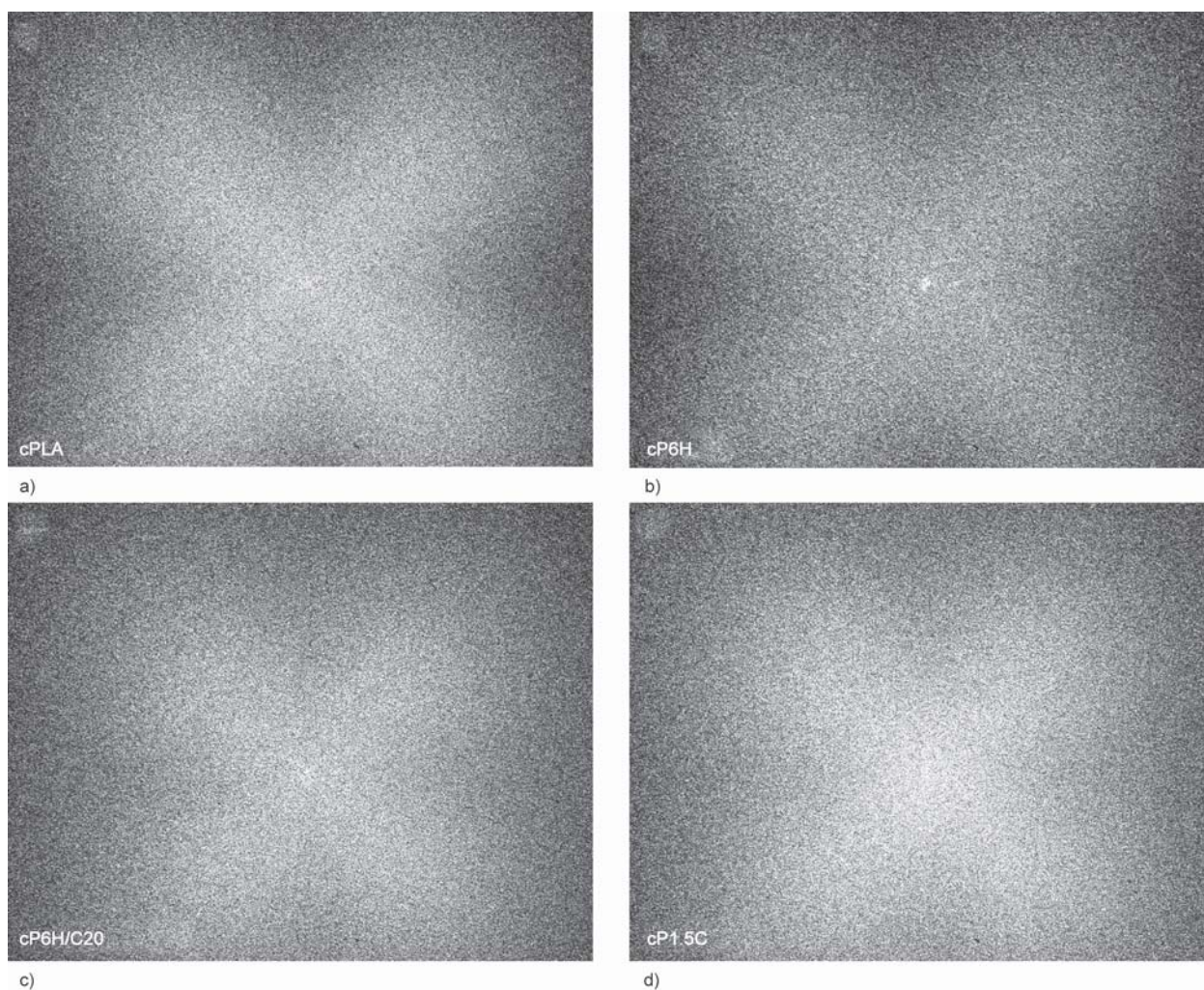


**Figure 3.** 2D-SALS Hv patterns of c-films: cPLA (a), cP6H (b), cP6H/C20 (c), and cP1.5C (d).

AFM analysis confirmed the presence of spherulites in neat PLA and cP6H, where fans of lamellae emanating from spherulite centers were clearly visible. On the contrary, parallel stacks of edge-on lamellae were observed in both rinsed cP6H/C20 and P1.5C. The average periodicity of lamellar structure in cPLA, cP6H was approx. 30–31 nm, whereas 20 and 23 nm in rinsed cP6H/C20 and rinsed cP1.5C, respectively. The depth of imprints left by EBS domains was approx. 0.1  $\mu\text{m}$ .

SEM and AFM analysis evidenced that the EBS layer strongly influenced PLA surface morphology formed during cold crystallization. EBS remained crystalline during cold crystallization of PLA, despite partial melting in that temperature range. Indeed, it is revealed elsewhere that EBS, which has two major crystalline forms, referred as alpha ( $\alpha$ ) and beta ( $\beta$ ), after thermal treatment at 120  $^{\circ}\text{C}$  contains mostly the alpha form [59]. Most probably, the peculiar morphology of PLA surface resulted from epitaxial

crystallization on EBS layer. According to Lotz' concept, epitaxial interaction between the nucleating agent and polymer [60, 61] is involved in the heterogeneous nucleation of polymers. It is worth mentioning that EBS activity in nucleating crystallization of PLA was already reported [*e.g.* 46, 47], which is suggestive of the epitaxial growth of PLA crystals. To the best of our knowledge, there are only a few reports on epitaxial crystallization of PLA, for instance on hexamethylbenzene substrate [62], on highly oriented polyethylene [63, 64], on oriented isotactic polypropylene [65]. It is worth noting that the edge-on orientation of lamellae with respect to foreign surfaces was frequently reported for thin polymer films, including nanolayers of polyolefins [66–68]. Such prevailing edge-on lamellae orientation was attributed to the nucleation of crystals induced by the parallel alignment of coil segments of molten polymer in contact with the hard walls [69]. However, in the present case, relatively large stacks of parallel

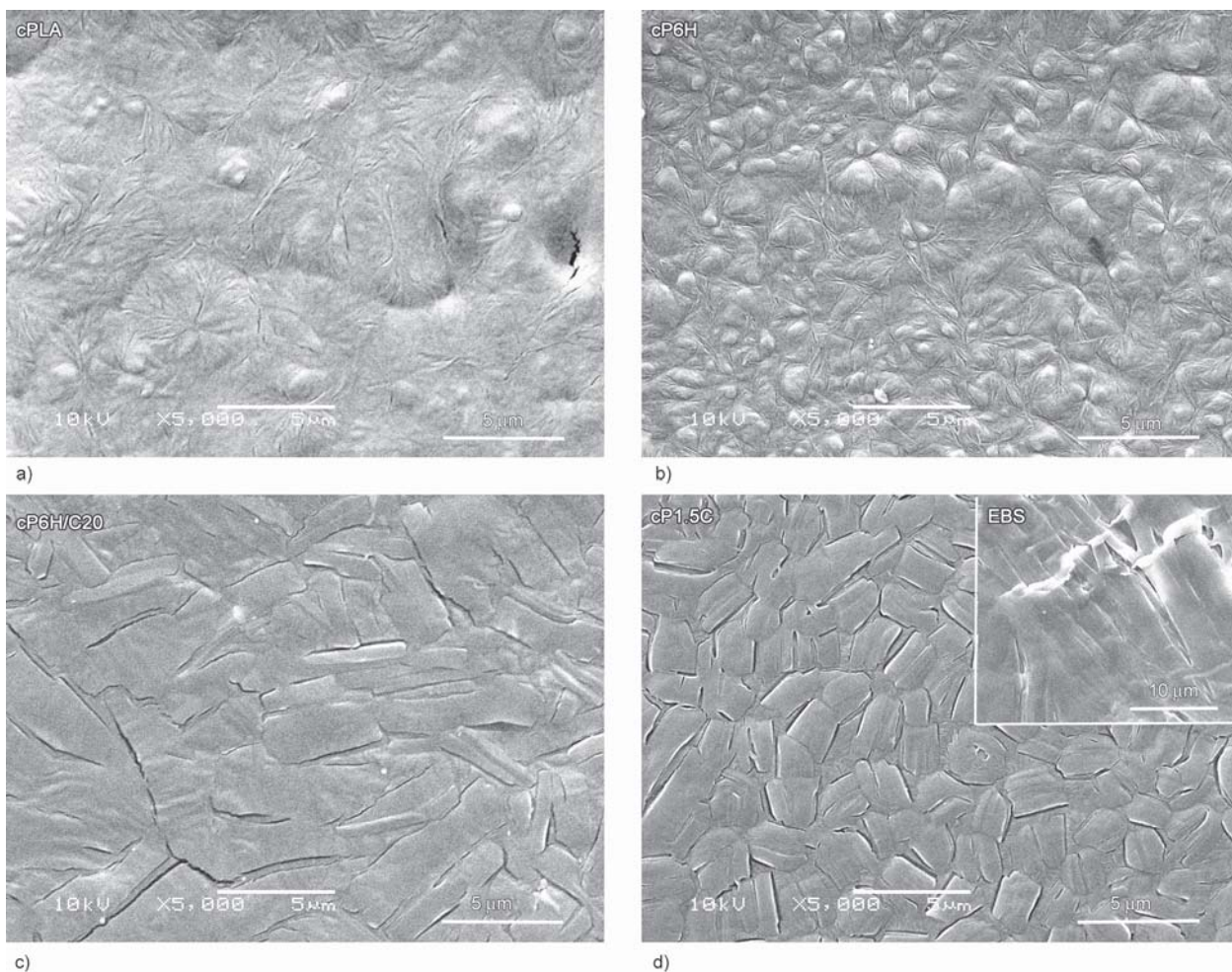


**Figure 4.** SEM micrographs of free surfaces of the c-films: cPLA (a), cP6H (b), cP6H/C20 (c) and cP1.5C (d). Inset shows the free surface of neat EBS.

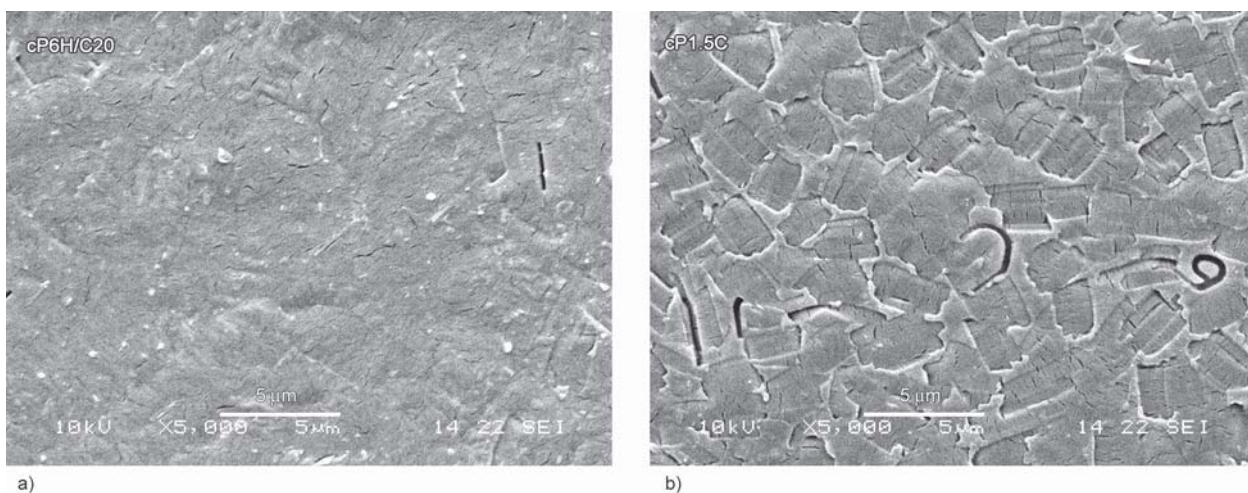


**Figure 5.** SEM micrographs of the free surfaces of rinsed films cP6H/C20 (a) and cP1.5C (b), after removal of EBS layers.

edge-on lamellae were observed, with sizes reflecting the sizes of EBS domains, and always well-aligned parallel to shorter sides of the domains. Such orientation strongly supports the conclusion of the epitaxial growth of PLA crystals on the EBS domains. The

lamellar orientation on PLA surface induced during cold crystallization by epitaxy on EBS is interesting from the point of view of the possibility of controlling the crystalline structure and orientation of crystallizable polymers [70], including PLA.

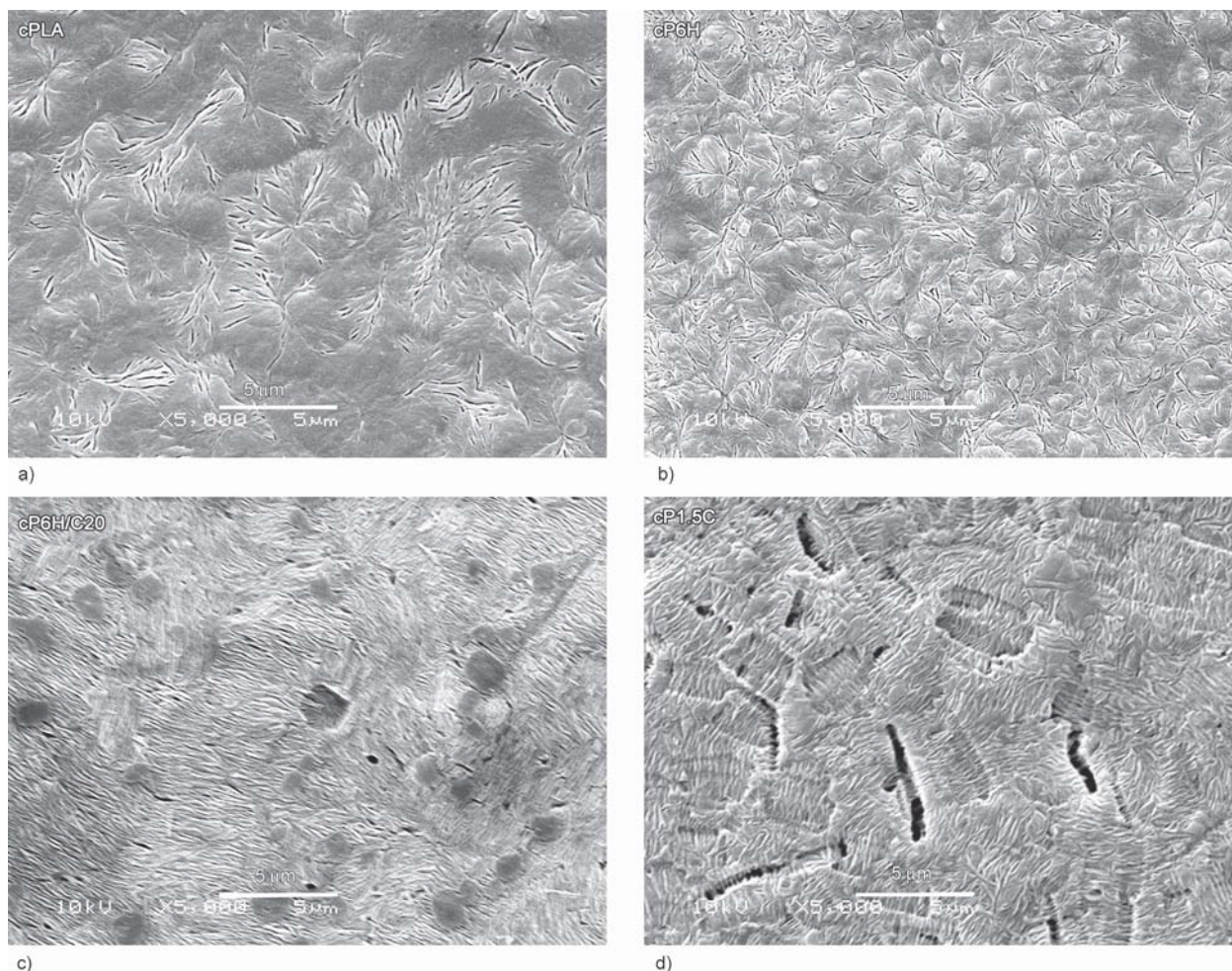


**Figure 6.** SEM images of the etched free surfaces of cPLA (a), cP6H (b), rinsed cP6H/C20 (c) and rinsed cP1.5C (d).

### 3.2.4. Surface wettability

Water contact angle (WCA) values of the materials studied are shown in Figure 8.

For neat cPLA film, WCA was  $70.7 \pm 1.2^\circ$ , while for cP6H film, it decreased to  $64.5 \pm 3.0^\circ$  due to the hydrophilic nature of HNT nanotubes [71] and their presence on the surface of this material. The increased wettability was also observed for PLA with similar content of HNT by others, *e.g.* [72, 73]. WCA of cP6H/C20 and cP1.5C increased to  $101.4 \pm 2.0^\circ$  and  $100.3 \pm 2.0^\circ$ , respectively, evidencing hydrophobicity of these materials [74]. Neat EBS was even more hydrophobic with WCA of  $124 \pm 3.0^\circ$ . The difference can originate from incomplete coverage of EBS-containing materials with the EBS layer. Another reason can be related to differences in surface roughness of EBS layers on those materials and pure EBS, as surface roughness also influences WCA values [75].

### 4. Conclusions

The surface morphology of crystalline PLA and PLA-based materials with different modifiers, HNT, EBS-modified HNT and EBS, was examined. The studied materials showed a glass transition temperature  $T_g$  approx.  $63^\circ\text{C}$  and crystallinity of about 37–40%. Surface of EBS-free materials, that is neat PLA and PLA nanocomposite with HNT, exhibited spherulitic structure. However, on surfaces of EBS-containing materials, that is PLA nanocomposite with EBS-treated HNT and PLA blend with EBS, thin EBS layers were found, with characteristic domain morphology. The layers were formed by EBS fraction that was exuded to surfaces of the molten materials during processing. Interestingly, PLA surface adjacent to the EBS layer crystallized in the form of stacks of parallel edge-on lamellae, different from spherulitic structure detected by SALS in the bulk of the materials. This was observed in PLA with

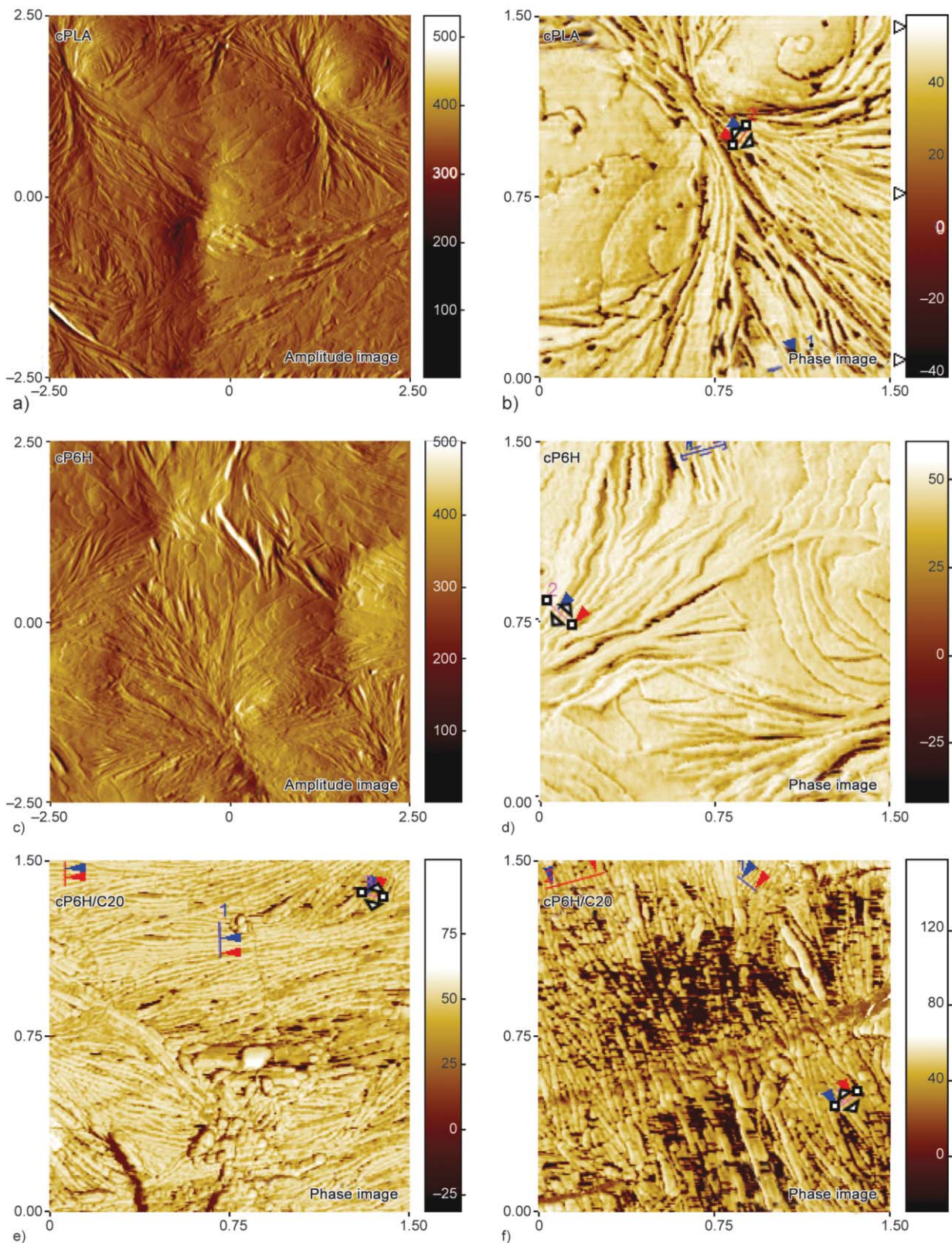


**Figure 7.** AFM amplitude and phase images of surfaces of cPLA (a) and (b), cP6H (c) and (d), rinsed cP6H/C20 (e) and rinsed cP1.5C (f). The axis scales are in micrometers. The places where periodicities of lamellae stacks were measured are marked with arrows.

EBS modified HNT and in the PLA blend with EBS. It is concluded that the edge-on lamella stacks grew epitaxially on the EBS layer. This effect has not been

observed in previous studies of EBS-containing PLA-based materials. It is worth emphasizing that the additives used modified water wettability of the

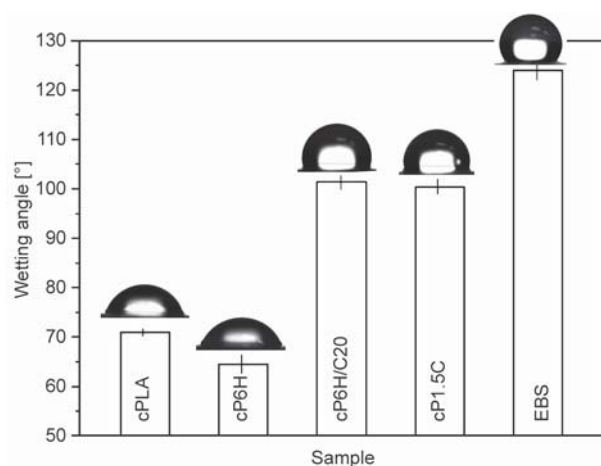


**Figure 8.** Water drops on free surfaces and corresponding WCA values of c-films: cPLA, cP6H, cP6H/C20, cP1.5C, and EBS.

materials. It was shown that HNT nanofiller enhanced hydrophilicity of PLA, while the EBS layers on surfaces imparted hydrophobicity. One can expect that the EBS layers on PLA based materials also alter other properties related to surface properties and structure, for instance, frictional.

### Acknowledgements

The study was conducted Under the Agreement on Scientific Cooperation between the Polish Academy of Sciences and the Fund for Scientific Research e FNRS (FRS -FNRS) Belgium. The statutory fund of the Centre of Molecular and Macromolecular Studies, Polish Academy of Sciences, and the Wallonia Region, Nord-Pas de Calais Region and European Community for the financial support in the frame of the IINTERREG IV – NANOLAC project, are kindly acknowledged.

### References

- [1] Nampoothiri K. M., Nair N. R., John R. P.: An overview of the recent developments in polylactide (PLA) research. *Bioresource Technology*, **101**, 8493–8501 (2010). <https://doi.org/10.1016/j.biortech.2010.05.092>
- [2] Drumright R. E., Gruber P. R., Henton D. E.: Polylactic acid technology. *Advanced Materials*, **12**, 1841–1846 (2000). [https://doi.org/10.1002/1521-4095\(200012\)12:23<1841::AID-ADMA1841>3.0.CO;2-E](https://doi.org/10.1002/1521-4095(200012)12:23<1841::AID-ADMA1841>3.0.CO;2-E)
- [3] Ren J.: *Biodegradable poly(lactic acid): Synthesis, modification, processing and applications*. Tsinghua University Press, Beijing, Springer, Berlin (2010). [https://doi.org/10.1007/978-3-642-17596-1\\_2](https://doi.org/10.1007/978-3-642-17596-1_2)
- [4] Piorkowska E.: Overview of biobased polymers. *Advances in Polymer Science*, **283**, 1–35 (2019). [https://doi.org/10.1007/12\\_2019\\_52](https://doi.org/10.1007/12_2019_52)
- [5] Dorgan J. R., Lehermeier H. J., Palade L-I., Cicero J.: Polyactides: Properties and prospects of an environmentally benign plastic from renewable resources. *Macromolecular Symposia*, **175**, 55–66 (2001). [https://doi.org/10.1002/1521-3900\(200110\)175:1<55::AID-MASY55>3.0.CO;2-K](https://doi.org/10.1002/1521-3900(200110)175:1<55::AID-MASY55>3.0.CO;2-K)
- [6] Masutani K., Kimura Y.: Present situation and future perspectives of poly(lactic acid). *Advances in Polymer Science*, **279**, 1–25 (2018). [https://doi.org/10.1007/12\\_2016\\_16](https://doi.org/10.1007/12_2016_16)
- [7] Kühnert I., Spörer Y., Brüning H., Tran N. H. A., Rudolph N.: Processing of poly(lactic acid). *Advances in Polymer Science*, **282**, 1–33 (2018). [https://doi.org/10.1007/12\\_2017\\_30](https://doi.org/10.1007/12_2017_30)
- [8] Malinconico M., Vink E. T. H., Cain A.: Applications of poly(lactic acid) in commodities and specialties. *Advances in Polymer Science*, **282**, 35–50 (2018). [https://doi.org/10.1007/12\\_2017\\_29](https://doi.org/10.1007/12_2017_29)
- [9] Bouzouita A., Notta-Cuvier D., Raquez J-M., Lauro F., Dubois P.: Poly(lactic acid)-based materials for automotive applications. *Advances in Polymer Science*, **282**, 177–219 (2018). [https://doi.org/10.1007/12\\_2017\\_10](https://doi.org/10.1007/12_2017_10)
- [10] Kowalczyk M., Piorkowska E., Dutkiewicz S., Sowinski P.: Toughening of polylactide by blending with a novel random aliphatic–aromatic copolyester. *European Polymer Journal*, **59**, 59–68 (2014). <https://doi.org/10.1016/j.eurpolymj.2014.07.002>
- [11] Krishnan S., Pandey P., Mohanty S., Nayak S. K.: Toughening of polylactic acid: An overview of research progress. *Polymer-Plastics Technology and Engineering*, **55**, 1623–1652 (2016). <https://doi.org/10.1080/03602559.2015.1098698>
- [12] Alias N. F., Ismail H.: An overview of toughening polylactic acid by an elastomer. *Polymer-Plastics Technology and Materials*, **58**, 1399–1422 (2019). <https://doi.org/10.1080/25740881.2018.1563118>
- [13] Jacobsen S., Fritz H. G.: Plasticizing polylactide—The effect of different plasticizers on the mechanical properties. *Polymer Engineering and Science*, **39**, 1303–1310 (1999). <https://doi.org/10.1002/pen.11517>
- [14] Murariu M., Da Silva Ferreira A., Pluta M., Bonnaud L., Alexandre M., Dubois P.: Polylactide (PLA)–CaSO<sub>4</sub> composites toughened with low molecular weight and polymeric ester-like plasticizers and related performances. *European Polymer Journal*, **44**, 3842–3852 (2008). <https://doi.org/10.1016/j.eurpolymj.2008.07.055>
- [15] Arias V., Höglund A., Odellius K., Albertsson A-C.: Polylactides with ‘green’ plasticizers: Influence of isomer composition. *Journal of Applied Polymer Science*, **130**, 2962–2970 (2013). <https://doi.org/10.1002/app.39446>

- [16] Pluta M., Piorkowska E.: Tough and transparent blends of polylactide with block copolymers of ethylene glycol and propylene glycol. *Polymer Testing*, **41**, 209–218 (2015).  
<https://doi.org/10.1016/j.polymertesting.2014.11.011>
- [17] Pluta M., Piorkowska E.: Tough crystalline blends of polylactide with block copolymers of ethylene glycol and propylene glycol. *Polymer Testing*, **46**, 79–87 (2015).  
<https://doi.org/10.1016/j.polymertesting.2015.06.014>
- [18] Zubrowska A., Piorkowska E., Bojda J.: Novel tough crystalline blends of polylactide with ethylene glycol derivative of POSS. *Journal of Polymers and the Environment*, **26**, 145–151 (2018).  
<https://doi.org/10.1007/s10924-016-0920-2>
- [19] Pluta M.: Melt compounding of polylactide/organoclay: Structure and properties of nanocomposites. *Journal of Polymer Science Part B: Polymer Physics*, **44**, 3392–3405 (2006).  
<https://doi.org/10.1002/polb.20957>
- [20] Pluta M., Jeszka J. K., Boiteux G.: Polylactide/montmorillonite nanocomposites: Structure, dielectric, viscoelastic and thermal properties. *European Polymer Journal*, **43**, 2819–2835 (2007).  
<https://doi.org/10.1016/j.eurpolymj.2007.04.009>
- [21] Raquez J-M., Habibi Y., Murariu M., Dubois P.: Polylactide (PLA)-based nanocomposites. *Progress in Polymer Science*, **38**, 1504–1542 (2013).  
<https://doi.org/10.1016/j.progpolymsci.2013.05.014>
- [22] Piekarska K., Sowinski P., Piorkowska E., Ul-Haque M. M., Pracella M.: Structure and properties of hybrid PLA nanocomposites with inorganic nanofillers and cellulose fibers. *Composites Part A: Applied Science and Manufacturing*, **82**, 34–41 (2016).  
<https://doi.org/10.1016/j.compositesa.2015.11.019>
- [23] Wu D., Wu L., Zhang M., Zhao Y.: Viscoelasticity and thermal stability of polylactide composites with various functionalized carbon nanotubes. *Polymer Degradation and Stability*, **93**, 1577–1584 (2008).  
<https://doi.org/10.1016/j.polymdegradstab.2008.05.001>
- [24] Wang Y., Lin C-S.: Preparation and characterization of maleated polylactide-functionalized graphite oxide nanocomposites. *Journal of Polymer Research*, **21**, 334/1–334/14 (2014).  
<https://doi.org/10.1007/s10965-013-0334-y>
- [25] Pluta M., Murariu M., Alexandre M., Galeski A., Dubois P.: Polylactide compositions. The influence of ageing on the structure, thermal and viscoelastic properties of PLA/calcium sulfate composites. *Polymer Degradation and Stability*, **93**, 925–931 (2008).  
<https://doi.org/10.1016/j.polymdegradstab.2008.02.001>
- [26] Pluta M., Murariu M., Dechief A-L., Bonnaud L., Galeski A., Dubois P.: Impact-modified polylactide-calcium sulfate composites: Structure and properties. *Applied Polymer Science*, **125**, 4302–4315 (2012).  
<https://doi.org/10.1002/app.36562>
- [27] Piekarska K., Piorkowska E., Bojda J.: The influence of matrix crystallinity, filler grain size and modification on properties of PLA/calcium carbonate composites. *Polymer Testing*, **62**, 203–209 (2017).  
<https://doi.org/10.1016/j.polymertesting.2017.06.025>
- [28] Murariu M., Doumbia A., Bonnaud L., Dechief A-L., Paint Y., Ferreira M., Campagne C., Devaux E., Dubois P.: High-performance polylactide/ZnO nanocomposites designed for films and fibers with special end-use properties. *Biomacromolecules*, **12**, 1762–1771 (2011).  
<https://doi.org/10.1021/bm2001445>
- [29] Busolo M. A., Lagaron J. M.: Antimicrobial biocomposites of melt-compounded polylactide films containing silver-based engineered clays. *Journal of Plastic Film and Sheeting*, **29**, 290–305 (2013).  
<https://doi.org/10.1177/8756087913478601>
- [30] Zhu A., Diao H., Rong Q., Cai A.: Preparation and properties of polylactide-silica nanocomposites. *Journal of Applied Polymer Science*, **116**, 2866–2873 (2010).  
<https://doi.org/10.1002/app.31786>
- [31] Vuluga Z., Corobea M. C., Elizetxea C., Ordonez M., Ghiurea M., Raditoiu V., Nicolae C. A., Florea D., Iorga M., Somoghi R., Trica B.: Morphological and tribological properties of PMMA/halloysite nanocomposites. *Polymers*, **10**, 816/1–816/23 (2018).  
<https://doi.org/10.3390/polym10080816>
- [32] Sabatini V., Taroni T., Rampazzo R., Bompieri M., Maggioni D., Meroni D., Ortenzi M. A., Ardizzone S.: PA6 and halloysite nanotubes composites with improved hydrothermal ageing resistance: Role of filler physicochemical properties, functionalization and dispersion technique. *Polymers*, **12**, 211/1–211/19 (2020).  
<https://doi.org/10.3390/polym12010211>
- [33] Sharma S., Singh A. A., Majumdar A., Butola B. S.: Harnessing the ductility of polylactic acid/ halloysite nanocomposites by synergistic effects of impact modifier and plasticiser. *Composites Part B: Engineering*, **188**, 107845/1–107845/10 (2020).  
<https://doi.org/10.1016/j.compositesb.2020.107845>
- [34] Wang S., Daelemans L., Fiorio R., Gou M., D'hooge D. R., De Clerck K., Cardon L.: Improving mechanical properties for extrusion-based additive manufacturing of poly(lactic acid) by annealing and blending with poly(3-hydroxybutyrate). *Polymers*, **11**, 1529/1–1529/13 (2019).  
<https://doi.org/10.3390/polym11091529>
- [35] Harris A. M., Lee E. C.: Improving mechanical performance of injection molded PLA by controlling crystallinity. *Journal of Applied Polymer Science*, **107**, 2246–2255 (2008).  
<https://doi.org/10.1002/app.27261>
- [36] Murariu M., Dechief A-L., Paint Y., Peeterbroeck S., Bonnaud L., Dubois P.: Polylactide (PLA)-halloysite nanocomposites: Production, morphology and key-properties. *Journal of Polymers and the Environment*, **20**, 932–943 (2012).  
<https://doi.org/10.1007/s10924-012-0488-4>

- [37] Gorrasi G., Pantani R., Murariu M., Dubois P.: PLA/halloysite nanocomposite films: Water vapor barrier properties and specific key characteristics. *Macromolecular Materials and Engineering*, **299**, 104–115 (2014). <https://doi.org/10.1002/mame.201200424>
- [38] Murariu M., Dechief A.-L., Ramy-Ratierison R., Paint Y., Raquez J.-M., Dubois P.: Recent advances in production of poly(lactic acid) (PLA) nanocomposites: A versatile method to tune crystallization properties of PLA. *Nanocomposites*, **1**, 71–82 (2015). <https://doi.org/10.1179/2055033214Y.0000000008>
- [39] Therias S., Murariu M., Dubois P.: Bionanocomposites based on PLA and halloysite nanotubes: From key properties to photooxidative degradation. *Polymer Degradation and Stability*, **145**, 60–69 (2017). <https://doi.org/10.1016/j.polyimdegradstab.2017.06.008>
- [40] Pluta M., Bojda J., Piorkowska E., Murariu M., Bonnaud L., Dubois P.: The effect of halloysite nanotubes and *N,N'*-ethylenebis(stearamide) on the properties of polylactide nanocomposites with amorphous matrix. *Polymer Testing*, **61**, 35–45 (2017). <https://doi.org/10.1016/j.polymertesting.2017.04.016>
- [41] Pluta M., Bojda J., Piorkowska E., Murariu M., Bonnaud L., Dubois P.: The effect of halloysite nanotubes and *N,N'*-ethylenebis(stearamide) on morphology and properties of polylactide nanocomposites with crystalline matrix. *Polymer Testing*, **64**, 83–91 (2017). <https://doi.org/10.1016/j.polymertesting.2017.09.013>
- [42] Nicolini K. P., Fukamachi C. R. B., Wypych F., Mangrich A. S.: Dehydrated halloysite intercalated mechanochemically with urea: Thermal behavior and structural aspects. *Journal of Colloid Interface Science*, **338**, 474–479 (2009). <https://doi.org/10.1016/j.jcis.2009.06.058>
- [43] Du M., Guo B., Jia D.: Newly emerging applications of halloysite nanotubes: A review. *Polymer International*, **59**, 574–582 (2010). <https://doi.org/10.1002/pi.2754>
- [44] Liu M., Zhang Y., Zhou C.: Nanocomposites of halloysite and polylactide. *Applied Clay Science*, **75–76**, 52–59 (2013). <https://doi.org/10.1016/j.clay.2013.02.019>
- [45] De Silva R. T., Pasbakhsh P., Goh K. L., Chai S.-P., Chen J.: Synthesis and characterisation of poly(lactic acid)/halloysite bionanocomposite films. *Journal of Composite Materials*, **48**, 3705–3717 (2014). <https://doi.org/10.1177/0021998313513046>
- [46] Nanthananon P., Seadan M., Pivsa-Art S., Suttiruwongwong S.: Enhanced crystallization of poly(lactic acid) through reactive aliphatic bisamide. *IOP Conference Series: Materials Science and Engineering*, **87**, 01206/1–01206/7 (2015). <https://doi.org/10.1088/1757-899X/87/1/012067>
- [47] Cai Y.-H.: Influence of ethylene bis-stearamide on crystallization behaviour of poly(L-lactide). *Asian Journal of Chemistry*, **25**, 6219–6221 (2013). <https://doi.org/10.14233/ajchem.2013.14326>
- [48] Saeidlou S., Huneault M. A., Li H., Park C. B.: Poly(lactic acid) crystallization. *Progress in Polymer Science*, **37**, 1657–1677 (2012). <https://doi.org/10.1016/j.progpolymsci.2012.07.005>
- [49] Zhang J., Yin H.-M., Chen C., Hsiao B. S., Yuan G.-P., Li Z.-M.: High-pressure crystallization of poly(lactic acid) with and without N<sub>2</sub> atmosphere protection. *Journal of Materials Science*, **48**, 7374–7383 (2013). <https://doi.org/10.1007/s10853-013-7552-x>
- [50] Sarasua J.-R., Prud'homme R. E., Wisniewski M., Le Borgne A., Spassky N.: Crystallization and melting behavior of polylactides. *Macromolecules*, **31**, 3895–3905 (1998). <https://doi.org/10.1021/ma971545p>
- [51] Zuza E., Ugartemendia J. M., Lopez A., Meaurio E., Lejardi A., Sarasua J.-R.: Glass transition behavior and dynamic fragility in polylactides containing mobile and rigid amorphous fractions. *Polymer*, **49**, 4427–4432 (2008). <https://doi.org/10.1016/j.polymer.2008.08.012>
- [52] Righetti M. C.: Amorphous fractions of poly(lactic acid). *Advances in Polymer Science*, **279**, 195–234 (2018). [https://doi.org/10.1007/12\\_2016\\_14](https://doi.org/10.1007/12_2016_14)
- [53] Tham W. L., Poh B. T., Ishak Z. A. M., Chow W. S.: Thermal behaviors and mechanical properties of halloysite nanotube-reinforced poly(lactic acid) nanocomposites. *Journal of Thermal Analysis and Calorimetry*, **118**, 1639–1647 (2014). <https://doi.org/10.1007/s10973-014-4062-2>
- [54] Pietrzak L., Piorkowska E., Galeski A., Bojda J., Sowinski P.: Modification of syndiotactic polypropylene with nano-calcium carbonate and halloysite. *International Polymer Processing*, **33**, 314–321 (2018). <https://doi.org/10.3139/217.3521>
- [55] Terzopoulou Z., Papageorgiou D. G., Papageorgiou G. Z., Bikiaris D. N.: Effect of surface functionalization of halloysite nanotubes on synthesis and thermal properties of poly( $\epsilon$ -caprolactone). *Journal of Materials Science*, **53**, 6519–6541 (2018). <https://doi.org/10.1007/s10853-018-1993-1>
- [56] Papageorgiou G. Z., Achilias D. S., Nanaki S., Beslikas T., Bikiaris D.: PLA nanocomposites: Effect of filler type on non-isothermal crystallization. *Thermochimica Acta*, **511**, 129–139 (2010). <https://doi.org/10.1016/j.tca.2010.08.004>
- [57] Stein R. S., Rhodes M. B.: Photographic light scattering by polyethylene films. *Journal of Applied Physics*, **31**, 1873–1884 (1960). <https://doi.org/10.1063/1.1735468>
- [58] Bartczak Z., Galeski A.: Homogeneous nucleation in polypropylene and its blends by small-angle light scattering. *Polymer*, **31**, 2027–2038 (1990). [https://doi.org/10.1016/0032-3861\(90\)90072-7](https://doi.org/10.1016/0032-3861(90)90072-7)
- [59] Rosen M., Franklin L. C.: Process for the interconversion of crystalline forms of ethylene bis-stearamide, U.S. Patent 4248792A, USA (1981).

- [60] Thierry A., Lotz B. A.: Epitaxial crystallization of polymers: Means and issues. in 'Handbook of polymer crystallization' (eds: Piorkowska E., Rutledge G. C.) Wiley, Hoboken, 237–286 (2013).  
<https://doi.org/10.1002/9781118541838.ch8>
- [61] Xin R., Zhang J., Sun X., Li H., Qiu Z., Yan S.: Epitaxial effects on polymer crystallization. *Advances in Polymer Science*, **277**, 55–94 (2017).  
[https://doi.org/10.1007/12\\_2015\\_329](https://doi.org/10.1007/12_2015_329)
- [62] Cartier L., Okihara T., Ikada Y., Tsuji H., Puiggali J., Lotz B.: Epitaxial crystallization and crystalline polymorphism of polylactides. *Polymer*, **41**, 8909–8919 (2000).  
[https://doi.org/10.1016/S0032-3861\(00\)00234-2](https://doi.org/10.1016/S0032-3861(00)00234-2)
- [63] An Y-K., Jiang S-D., Yan S-K., Sun J-R., Chen X-S.: Crystallization behavior of polylactide on highly oriented polyethylene thin films. *Chinese Journal of Polymer Science*, **29**, 513–519 (2011).  
<https://doi.org/10.1007/s10118-010-1028-0>
- [64] Tu C., Jiang S., Li H., Yan S.: Origin of epitaxial cold crystallization of poly(L-lactic acid) on highly oriented polyethylene substrate. *Macromolecules*, **46**, 5215–5222 (2013).  
<https://doi.org/10.1021/ma400743k>
- [65] Guan G., Zhang J., Sun X., Li H., Yan S., Lotz B.: Oriented overgrowths of poly(L-lactide) on oriented isotactic polypropylene: A sequence of soft and hard epitaxies. *Macromolecular Rapid Communication*, **39**, 1800353/1–1800353/6 (2018).  
<https://doi.org/10.1002/marc.201800353>
- [66] Jin Y., Rogunova M., Hiltner A., Baer E., Nowacki R., Galeski A., Piorkowska E.: Structure of polypropylene crystallized in confined nanolayers. *Journal of Polymer Science Part B Polymer Physics*, **42**, 3380–3396 (2004).  
<https://doi.org/10.1002/polb.20211>
- [67] Bernal-Lara T. E., Masirek R., Hiltner A., Baer E., Piorkowska E., Galeski A.: Morphology studies of multilayered HDPE/PS system. *Journal of Applied Polymer Science*, **99**, 597–612 (2006).  
<https://doi.org/10.1002/app.22178>
- [68] Langhe D. S., Hiltner A., Baer E.: Melt crystallization of syndiotactic polypropylene in nanolayer confinement impacting structure. *Polymer*, **52**, 5879–5889 (2011).  
<https://doi.org/10.1016/j.polymer.2011.10.018>
- [69] Ma Y., Hu W., Reiter G.: Lamellar crystal orientations biased by crystallization kinetics in polymer thin films. *Macromolecules*, **39**, 5159–5164 (2006).  
<https://doi.org/10.1021/ma060798s>
- [70] Wittmann J. C., Lotz B.: Epitaxial crystallization of polymers on organic and polymeric substrates. *Progress in Polymer Science*, **15**, 909–948 (1990).  
[https://doi.org/10.1016/0079-6700\(90\)90025-V](https://doi.org/10.1016/0079-6700(90)90025-V)
- [71] Meng Y., Wang M., Tang M., Hong G., Gao J., Chen Y.: Preparation of robust superhydrophobic halloysite clay nanotubes via mussel-inspired surface modification. *Applied Sciences*, **7**, 1129–1146 (2017).  
<https://doi.org/10.3390/app7111129>
- [72] Alakrach A. M., Noriman N. Z., Dahham O. S., Hamzah R., Alsaadi M. A., Shayfull Z., Idrus S. Z. S.: Chemical and hydrophobic properties of PLA/HNTs-ZrO<sub>2</sub> bio-nanocomposites. *Journal of Physics: Conference Series*, **1019**, 012065/1–012065/6 (2018).  
<https://doi.org/10.1088/1742-6596/1019/1/012065>
- [73] Nizar M. M., Hamzah M. S. A., Razak S. I. A., Nayan N. H. M.: Thermal stability and surface wettability studies of polylactic acid/halloysite nanotube nanocomposite scaffold for tissue engineering studies. *IOP Conference Series: Materials Science and Engineering*, **318**, 012006/1–012006/8 (2018).  
<https://doi.org/10.1088/1757-899X/318/1/012006>
- [74] Law K-Y.: Definitions for hydrophilicity, hydrophobicity, and superhydrophobicity: Getting the basics right. *The Journal of Physical Chemistry Letters*, **5**, 686–688 (2014).  
<https://doi.org/10.1021/jz402762h>
- [75] Bhushan B., Nosonovsky M.: The rose petal effect and the modes of superhydrophobicity. *Philosophical Transactions of the Royal Society A: Mathematical, Physical and Engineering Sciences*, **368**, 4713–4728 (2010).  
<https://doi.org/10.1098/rsta.2010.0203>